

Understanding Jupiter's Interior

Burkhard Militzer^{1,2}, François Soubiran¹, Sean M. Wahl¹, William Hubbard³

¹Department of Earth and Planetary Science, University of California, Berkeley, CA 94720, USA.

²Department of Astronomy, University of California, Berkeley, CA 94720, USA.

³Lunar and Planetary Laboratory, University of Arizona, Tucson, AZ 85721, USA.

Abstract. This article provides an overview of how models of giant planet interiors are constructed. We review measurements from past space missions that provide constraints for the interior structure of Jupiter. We discuss typical three-layer interior models that consist of a dense central core and an inner metallic and an outer molecular hydrogen-helium layer. These models rely heavily on experiments, analytical theory, and first-principle computer simulations of hydrogen and helium to understand their behavior up to the extreme pressures ~ 10 Mbar and temperatures $\sim 10\,000$ K. We review the various equations of state used in Jupiter models and compare them with shock wave experiments. We discuss the possibility of helium rain, core erosion and double diffusive convection may have important consequences for the structure and evolution of giant planets. In July 2016 the *Juno* spacecraft entered orbit around Jupiter, promising high-precision measurements of the gravitational field that will allow us to test our understanding of gas giant interiors better than ever before.

1. Introduction

In this article, we will provide a brief overview of how models for the interiors of giant planets are put together. While much of this discussion applies to all giant planets, this article will be focused on Jupiter in particular. We will review results from space missions that visited the planet earlier and then we will discuss what we expect from the *Juno* mission presently in orbit around Jupiter.

All giant planet interior models rely on an equation of state that describes how materials behave under the extreme pressure (~ 10 Mbar) and temperature ($\sim 10\,000$ K) conditions in planetary interiors. So in section 3, we compare the results from laboratory experiments, semi-analytical EOS models and *ab initio* simulations of dense hydrogen and of helium. In section 4, we review experimental and theoretical predictions for the properties of hydrogen-helium mixtures. We discuss *ab initio* simulations that focused on the question whether hydrogen-helium mixtures phase separate at high pressure, where hydrogen becomes a metallic fluid while helium remains in an insulating state. This process may lead to helium rain in the interior of giant planets, which has been invoked by *Stevenson and Salpeter* [1977a, b] to explain Saturn's unusually large infrared emissions.

In section 5, we compare the prediction for Jupiter's temperature-pressure profiles and discuss various interior models. In section 6, we compare adiabatic and super-adiabatic models, revisit the question of whether present day Jupiter has dense central core and if a primordial core could be partially or fully eroded.

2. Interior Constraints from Past Space Missions

Over the past 43 years Jupiter has been visited by nine spacecraft. Out of these missions the primary contributions to our understanding of Jupiter's interior were made by the *Pioneer 10 & 11* fly-bys, the *Voyager 1 & 2* fly-bys and the

Galileo orbiter. In July 2016, the *Juno* spacecraft entered a low-periapse orbit, in order to provide the most precise measurement of Jupiter's gravitational field to date, as well as better constraints on the composition of the outer envelope.

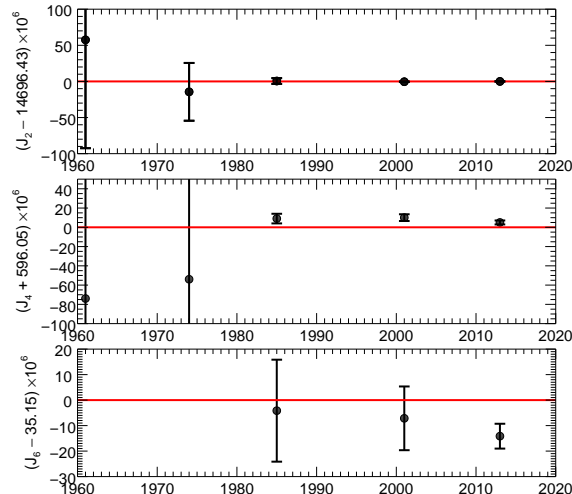


Figure 1. Improvement in measurements of Jupiter's first even zonal harmonics, as a function of year (abscissa). All J_n values are normalized to $a = 71492$ km, and referenced to theoretical values from a recent Jupiter model [Hubbard and Militzer, 2016], horizontal red line.

The most direct constraints on Jupiter's interior structure comes from measurements of the non-radial terms in its external gravitational potential. Jupiter's large surface oblateness (second only to Saturn's in the solar system) is a visible manifestation of its rapid rotation rate and low mean density. Correspondingly, the planet's external gravitational potential has large zonal harmonic coefficients J_n , which can be measured by modeling their effects on the orbit of a nearby spacecraft or natural satellite. These coefficients are weighted integrals over the interior density distribution

arXiv:1608.02685v1 [astro-ph.EP] 9 Aug 2016

$\rho(\mathbf{r})$,

$$J_n = -\frac{2\pi}{Ma^n} \int dr d\mu \rho(\mathbf{r}) r^{n+2} P_n(\mu), \quad (1)$$

where M is Jupiter's mass, a is a normalizing radius (usually taken to be the equatorial radius at a pressure of 1 bar, 71492 km), $\mu = \sin L$ (L is the planetocentric latitude), $P_n(\mu)$ are Legendre polynomials, and r is the radial distance from the planet's center. To relate given values of J_n to interior structure, we assume that the planet is everywhere in hydrostatic equilibrium in its rotating frame, and that a unique barotrope $P = P(\rho)$ relates the pressure P and the mass density ρ . Thus, a model of Jupiter using a barotrope that reproduces the external gravity terms is an acceptable one.

The J_2 term in the harmonic expansion is mostly Jupiter's interior's linear response to rotation, but higher-order terms J_n arise entirely from nonlinear response, and require careful numerical modeling to properly test an assumed interior barotrope [Zharkov and Trubitsyn, 1978]. The higher-order terms are difficult to measure at a significant distance from Jupiter since the gravitational potential contribution from a given zonal harmonic J_n varies as $(a/r)^{n+1}$. Prior to the first spacecraft measurements at Jupiter in 1973, our only information about J_n came from ground-based observations of satellite motions. Fig. 1 exhibits the dramatic improvement in measurements of the J_n over the last ~ 50 years.

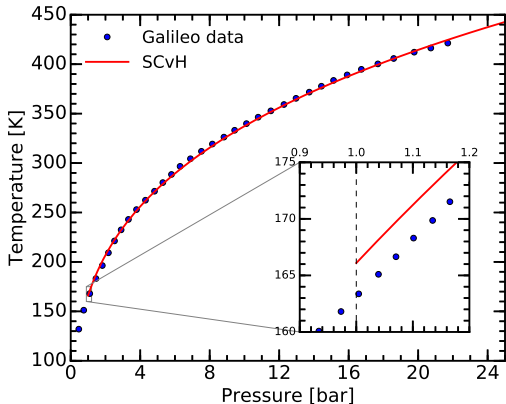


Figure 2. Comparison of Galileo entry probe T - P measurements [Galileo] with Saumon et al. [1995] EOS model. For the latter calculation, we assumed a dry adiabat with helium mass fraction of 0.247 a starting from a temperature of 166.1 K at 1 bar.

2.1. Pioneer and Voyager Missions

Pioneers 10 and 11 were the first spacecraft to reach the vicinity of Jupiter, in December 1973 and December 1974. These spacecraft executed hyperbolic flyby orbits with periapses at $2.8a$ and $1.6a$ respectively, permitting an improved determination of J_2 and J_4 , but the signal from higher-order terms was not measurable. *Voyagers* 1 and 2 executed Jupiter flybys in March 1979 and 1979, with periapses of $4.9a$ and $10.1a$ respectively. Thus, the *Pioneer* flybys were more sensitive to terms above J_2 [Campbell and Synnott, 1985].

2.2. Galileo Mission and Entry Probe

The *Galileo* spacecraft arrived at Jupiter in December 1995, and remained in orbit around Jupiter for 8 years. The main *Galileo* spacecraft did not make a large contribution to

improvements in measurements of Jupiter's J_n , although it made important measurements of the corresponding terms in the external gravity of the Galilean satellites.

Galileo's most significant contribution to the understanding of Jupiter's interior was deploying an entry probe that measured the structure and composition of Jupiter's near-equatorial atmosphere to a maximum pressure of 22 bar [Seiff et al., 1998]. The entry probe data are fundamental as an initial condition for constraining the Jovian interior barotrope. Conservatively estimated, the probe's sensors were able to measure temperature with a precision varying from 0.1 K at 100 K to 1 K at 500 K [Magalhães et al., 2002]. Seiff et al. [1998] inferred an uncertainty of less than 2% for probe's pressure measurements by performing an *a posteriori* calibration that was needed because the temperature exceeded the original calibration range. Based on these results, Seiff et al. [1998] fitted a dry adiabatic profile with a temperature of 166.1 K at 1 bar, which we reproduced in Fig. 2 with a H-He isentrope derived from the Saumon et al. [1995] EOS model. We find a good agreement overall between the theoretical H-He isentrope and the measured data but is a not a perfect match. For example there is deviation of approximately 2 K at starting point of 1 bar.

The *Galileo* entry probe further constrained the composition along the barotrope, showing the outer layers of Jupiter to have a composition that is not too different from that of the sun. The probe measured a helium mass fraction of $Y = 0.23$ and a mass fraction of heavier elements of $Z \approx 0.017$. The heavy element component was primarily comprised of the hydrides H_2O , CH_4 , and NH_3 [Wong et al., 2004]. It is important to note that the probe value of Y is below the protosolar value of 0.274 [Lodders, 2003], providing evidence of helium sequestration in Jupiter's interior. The probe's measurement of a strong neon depletion with respect to protosolar abundance was further evidence of helium rain [Wilson and Militzer, 2010].

2.3. Combined Analysis from Past Missions

The next spacecraft to visit Jupiter was *Ulysses*, which executed a flyby in February 1992 at $6.3a$. Optimized to study the solar wind, *Ulysses* did not contribute significantly to Jovian interior constraints. Subsequent encounters by *Cassini-Huygens* in December 2000 and by *New Horizons* between January and may 2007, did not afford opportunities to significantly improve measurements of Jupiter's gravitational field.

During the long interval before the expected arrival of the Juno orbiter in 2016, R. A. Jacobson [Jacobson, 2001, 2003, 2013] has synthesized disparate data sets including Earth-based astrometry, satellite mutual eclipses and occultations, and satellite eclipses by Jupiter, as well as spacecraft data from Doppler tracking, radiometric range, very-long baseline interferometry, radio occultations, and optical navigation imaging from *Pioneer* 10 & 11, *Voyager* 1 & 2, *Ulysses*, *Galileo*, and *Cassini*. More recent data points shown in Fig. 1 reflect this work.

2.4. Juno Mission

The Juno spacecraft, launched in 2011 and inserted in Jupiter's orbit on July 4, 2016, is optimized for measurements to constrain Jupiter's interior structure. More than 20 polar orbits with 14-day periods and periapses at $\sim 1.07a$ will be devoted to X - and $K\alpha$ -band measurements of spacecraft motions in Jupiter's gravity potential, with an expected line-of-sight velocity precision $\sim 2\mu\text{m/s}$. Terms in Jupiter's gravitational potential to $\sim J_{10}$ should be measurable, along with Jupiter's second-degree tidal response to its nearest large satellites. Predicted values of Jupiter's J_2 , J_4 , and J_6 are shown in Fig. 1; predictions of J_8 and J_{10} are

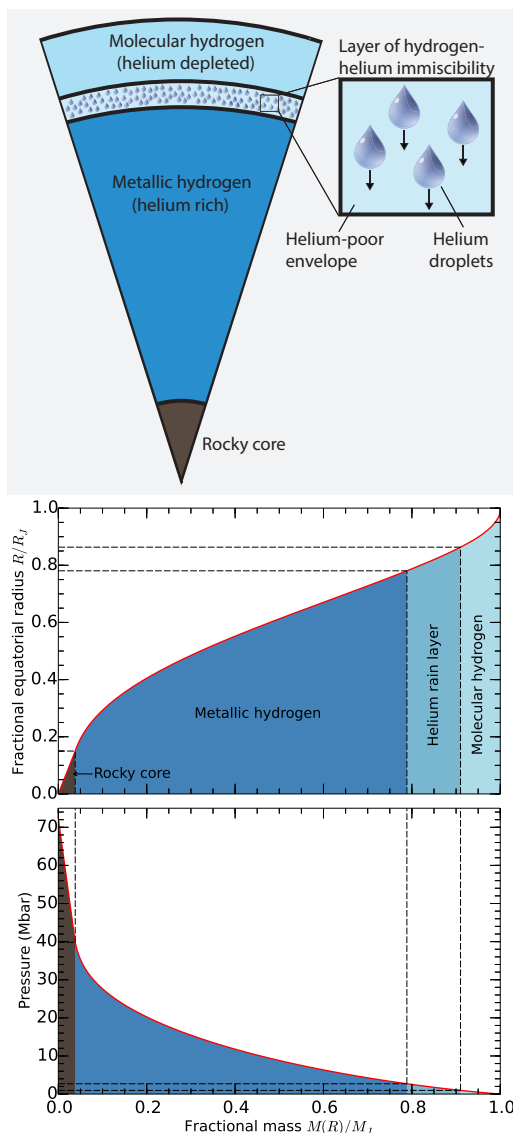


Figure 3. The upper diagram shows a model of Jupiter’s interior with the hydrogen-helium immiscibility layer. Lower two diagrams show the fractional radius and pressure as a function of fractional mass according to *Hubbard and Militzer* [2016].

also published [*Hubbard and Militzer*, 2016]. Predicted values of Jupiter’s tidal Love numbers [*Wahl et al.*, 2016a, b] are available for comparison with the tidal measurements. The precision of predictions and expected measurements is such that relative discrepancies at the level of $\sim 10^{-7}$ would be detectable. Gravity anomalies attributable to Jovian interior dynamics, apart from purely hydrostatic response, may produce a detectable signal [*Kaspi and Galanti*, 2016].

Over the expected mission lifetime of ~ 20 months, a sufficient arc of the angular precession of Jupiter’s spin axis should be measurable to yield a meaningful result for Jupiter’s spin angular momentum, $L = C\omega$, where C is Jupiter’s axial moment of inertia and ω is the spin rate. If the relevant ω is the well-known and stable value for Jupiter’s magnetic field, virtually any interior model fitted to J_2 predicts $C = 0.26Ma^2$ [*Hubbard and Militzer*, 2016]. Measurement of an L significantly different from the value implied by Jupiter’s magnetic field rotation rate would suggest differential rotation involving a substantial fraction of the planetary mass.

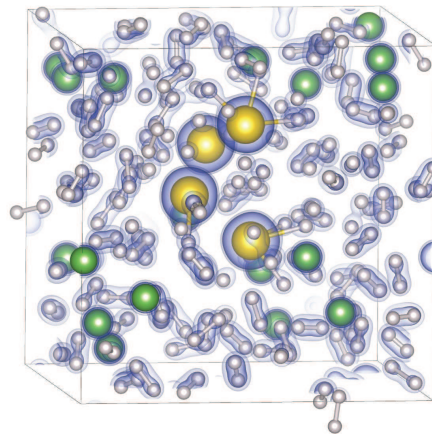


Figure 4. Snapshot from a DFT-MD simulation of 220 hydrogen, 18 helium, and 4 iron atoms that were introduced as an example of heavier elements [*Soubiran and Militzer*, 2016]. The grey isosurfaces represent the density of valence electrons. Periodic boundary conditions were used to mimic a macroscopic system.

The microwave radiometer (MWR) experiment on Juno will probe abundances of the condensable gases H_2O , NH_3 , and H_2SO_4 by sounding Jupiter’s deep atmosphere at six wavelengths from 1.37 to 50 cm, with sensitivity to levels at pressures ranging from ~ 1 bar to ~ 100 bar [*Janssen et al.*, 2014]. Although results from MWR may confirm the Galileo probe value for a metallicity $Z \approx 0.017$ in the outermost region of the jovian barotrope, a significant change in the metallicity would change the inferred mass density of Jupiter’s outer layers with repercussions on jovian structure at deeper layers.

3. Equations of State of Hydrogen and Helium

3.1. Theory, Simulations, and Shock Wave Experiments of Dense Hydrogen

Hydrogen is the most common element in the universe. Hydrogen and helium are the dominant elements in the interiors of main-sequence stars and gas giant planets. Because of this astrophysical context, the equation of state (EOS) of hydrogen has been studied with various methods for many decades. Here we will review a selected set of articles that contributed to our understanding of dense, molecular hydrogen in the outer envelope of giant planets as well as of metallic hydrogen in their deep interior (Fig. 3). Because Jupiter has a strong, dipolar magnetic field, we know conducting, metallic hydrogen must be present in its interior.

Long before laboratory experiments or *ab initio* computer simulations became available, the EOS of dense hydrogen plasma was characterized with analytical free energy models [*Ebeling et al.*, 1991] that invoke the *chemical picture*. In this approach, one describes plasmas as a collection of charged ions and electrons as well as neutral particle such as molecules and atoms. Approximate free energy functions are derived for each species and the chemical composition is obtained by minimizing the combined free energy for a given pressure and temperature.

Chemical models are known to work very well in regimes of weak interaction. At low density, the ionization equilibrium can be derived from the ideal Saha equation [*Fowler and Guggenheim*, 1965], which neglects all interactions.

Various elaborate analytical schemes have been derived to introduce interaction effects into free energy models. Not all of these were constructed to describe the whole high-temperature phase diagram as done by *Saumon and Chabrier* [1992]. *Ebeling and Richert* [1985b] studied the plasma and the atomic regime, while models by *Beule et al.* [1999] and *Bunker et al.* [1997] were designed to describe the dissociation of molecules. The *Ross* [1998] model was primarily developed to study the molecular-metallic transition. One difficulty common to free energy models is how to treat the interaction of charged and neutral particles. Often, this is done by introducing hard-sphere radii and additional corrections. These kinds of approximations lead to discrepancies between various chemical models. The differences are especially pronounced in the regime of the molecular-to-metallic transition because of the high density and the presence of neutral and charged species. If the derivatives of the free energy are continuous in this regime, a gradual molecular-to-metallic transition is predicted. If, on the

other hand, the different components of the free energy lead to discontinuous first derivatives, a first-order transition, or plasma phase transition (PPT) is inevitably predicted.

The question whether such PPT exists remains controversial. Many models have predicted a PPT with a critical point and coexistence region of two fluids characterized by different degrees of ionization and densities. A PPT was first placed on the hydrogen phase diagram by *Landau and Zeldovich* [1943]. First calculations have been made by *Norman and Starostin* [1968] and *Ebeling and Sändig* [1973]. A number of different free energy models such as those by [*Saumon and Chabrier*, 1992; *Kitamura and Ichimaru*, 1998; *Beule et al.*, 1999] predict a PPT. The exact location of the critical point and the coexistence region differ considerably and other models show continuous transitions [*Ross*, 1998]. Since this was an open question, [*Saumon and Chabrier*, 1992] provided an alternate model where they smoothly interpolate between both regimes.

Path integral Monte Carlo simulations by *Magro et al.* [1996] showed evidence of a first order transition in dense hydrogen. However, it was predicted to occur at relatively low temperatures [*Militzer and Graham*, 2006], for which PIMC results showed some dependence on the choice of fermion nodes. In this temperature regime, density functional molecular dynamics (DFT-MD) simulations work very efficiently. A snapshot from such simulations is shown in Fig. 4. Simulations by *Vorberger et al.* [2007] and *Militzer et al.* [2008] predicted a gradual molecule-to-metallic transition for temperature conditions in the interiors of Jupiter and Saturn. However, at lower temperatures (< 2000 K), well below the giant planet interior adiabats, DFT-MD simulations also predict a first-order transition [*Morales et al.*, 2010; *Lorenzen et al.*, 2011].

Significant progress has been made with high pressure laboratory experiments since the reverberating shock wave measurements by *Weir et al.* [1996] first produced hot, metallic hydrogen in the laboratory. Still it has remained a challenge to determine whether the molecular-to-metallic transition is of first-order. Measurements by *Fortov et al.* [2007] and most recently by *Knudson et al.* [2015] both showed evidence of a first-order transition. Still more work is needed to reconcile the results from different experiments with each other and develop a consistent theoretical framework.

The existence of a first-order molecular-to-metallic transition at sufficiently high temperature could introduce a convective barrier into Jupiter's interior. It would thus delay cooling of its interior and stabilize a compositional difference between the molecular and metallic layers. Such a difference is indeed invoked in most models for Jupiter's interior in order to match the gravitational moment J_4 but the origin of this difference remain poorly understood. We favor the hypothesis that the convective barrier was instead introduced by helium rain, which we will discuss in section 4.2. For the interior models discussed later in this article, we will rely on DFT-MD simulations that predict a gradual molecular-to-metallic transition for pure hydrogen for the temperatures in Jupiter's interior.

While unanswered questions remain regarding the phase diagram of dense hydrogen, significant progress has been made in characterizing the shock Hugoniot curve of hydrogen, which is summarized in Fig. 5. Shock wave experiments are the preferred laboratory technique [*Zeldovich and Raizer*, 1968] to determine the equation of state at high pressure and temperature. During such experiments, a driving force is utilized to propel a pusher at constant velocity U_p into a material at predetermined initial conditions ($\rho_0 = m/V_0, P_0, T_0$). The impact generates a planar shock wave, which travels at the constant velocity U_s , where $U_s > U_p$. Behind the shock wave, the material reaches

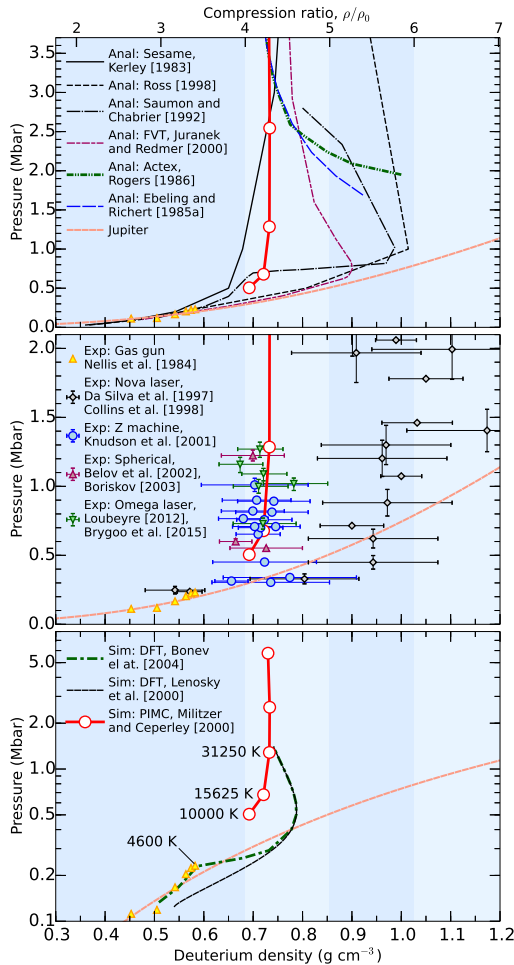


Figure 5. Comparison of the deuterium shock Hugoniot curves derived with semi-analytical methods (upper panel: *Rogers* [1986], *Ebeling and Richert* [1985a], *Saumon and Chabrier* [1992], *Kerley* [1983], *Juranek and Redmer* [2000], *Ross* [1998]), shock wave experiments (middle panel: *Nellis et al.* [1984], *Da Silva et al.* [1997], *Collins et al.* [1998], *Knudson et al.* [2001], *Belov et al.* [2002], *Boriskov* [2003]), and first-principles computer simulations (lower panel: [*Militzer and Ceperley*, 2000], [*Lenosky et al.*, 2000], *Bonev et al.* [2004]). Changes in background color mark densities equal to 4, 5, and 6 times the initial deuterium density of $\rho_0 = 0.17 \text{ g cm}^{-3}$.

a final state thermodynamic equilibrium ($\rho = m/V, P, T$). The conservation laws of mass, momentum, and energy, E , across the shock interface leads to the Rankine-Hugoniot equations [Rankine, 1870; Hugoniot, 1887, 1889], which have been discussed in detail by Zeldovich and Raizer [1968],

$$P = \varrho_0 U_s U_p + P_0 \quad (2)$$

$$\rho = \rho_0 \frac{U_s}{U_s - U_p} \quad (3)$$

$$R(\rho, T) = E - E_0 + \frac{1}{2}(V - V_0)(P + P_0) = 0 \quad (4)$$

It is remarkable that the measurements of just U_s and U_p allow for an absolute EOS measurement. The shock temperature, however, must be determined independently. The shock Hugoniot curve in Fig. 5 emerges as collection of final states for different U_p . The computation of this curve is straightforward. For a theoretical EOS provided in term of $E(\rho, T)$ and $P(\rho, T)$, one uses Eq. 4 to solve for $R(\rho, T) = 0$ by varying ρ at fixed T .

In Fig. 5, we compare the experimental Hugoniot curves with predictions from analytical techniques and first-principles computer simulations based on PIMC and DFT-MD. Because of shock heating, the temperature along shock Hugoniot curve rise significantly more rapidly than that on an adiabat, which makes it difficult to relate shock wave measurements to planetary interiors [Militzer and Hubbard, 2007]. In P - ρ space, the Hugoniot curves plot at higher pressures than Jupiter's adiabat. Nevertheless, these measurements provide invaluable constraints for the theoretical EOS calculations.

In the upper panel of Fig. 5, we compare various analytical EOS models. In the limits of high pressure, all curves are expected to converge to 4-fold compression, the limiting case for a non-relativistic gas ($\rho/\rho_0 = 4$). The activity expansion (ACTEX) by Rogers [1986], the Padé approximations in the chemical picture by Ebeling and Richert [1985a] and Saumon and Chabrier [1992] EOS model all predict compression ratio of ~ 5.5 at 2 Mbar and then converged to limit of 4-fold compression at higher pressure. The Sesame model by Kerley [1983], which has been used frequently to simulate a variety of shock processes, predicts a lower shock compression in comparison. The fluid variational theory (FVT) by Juránek and Redmer [2000] yield compression ratios up to 5.2. The linear mixing model by Ross [1998] stands out among all EOS models because it predicts shock compression ratios between 5.5 and 6.0 in the entire pressure interval from 1 to 4 Mbar.

When laser-driven shock wave experiments by Da Silva et al. [1997] and Collins et al. [1998] generated megabar pressures in deuterium for the first time, the results were surprising because they implied shock compression ratios of ~ 6 and therefore favored the linear mixing model by Ross [1998]. These measurements sparked an intense debate in the high-pressure community and motivated additional experimental and theoretical work. Points of concern were that neither the PIMC simulations [Militzer and Ceperley, 2000] nor the DFT-MD simulations [Lenosky et al., 2000] could reproduce the results from laser-driven shock measurements. Later DFT-MD simulations by Bonev et al. [2004], that treated the molecular phase more accurately, improved the agreement with the gas-gun shock wave experiments by Nellis et al. [1984] below 0.25 Mbar but the results at higher pressure remained unchanged. The agreement between the two first-principle simulation methods, PIMC and DFT-MD, is reasonably good, though not yet perfect. This made it possible to put together consistent EOS tables for hydrogen [Militzer and Ceperley, 2001], helium [Militzer, 2009], carbon [Benedict et al., 2014], nitrogen [Driver and Militzer, 2016], oxygen [Driver et al., 2015], water [Driver and Militzer, 2012], neon [Driver and Militzer,

2015], and most recently silicon [Militzer and Driver, 2015]. In each case, results from PIMC simulations that are very efficient at high temperature were combined with DFT-MD results at low temperature.

A major contribution towards resolving the controversy regarding the deuterium Hugoniot curve came from magnetically driven shock experiments by Knudson et al. [2001], which favor a maximum shock compression ratio of ~ 4.3 , broadly consistent with predictions from first-principles simulations. Later, similar results were reported from spherically converging shock wave experiments by Belov et al. [2002] and by Boriskov [2003] as well as by planar shock wave experiments by Brygoo et al. [2015] that were performed at the Omega laser facility. Because of all three new measurements favor a compression of ~ 4.3 , in keeping with first-principles simulations, one may regard the controversy around the deuterium Hugoniot curve to be resolved with satisfactory accuracy. If we adopt this view, however, then Saumon et al. [1995] EOS would be no longer the best EOS to model giant planet interiors because it deviates from shock measurements for $P > 0.7$ Mbar.

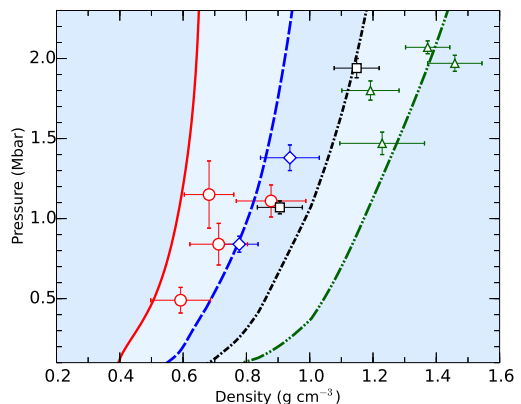


Figure 6. Comparison of the helium shock Hugoniot curve derived DFT-MD simulations (lines, Militzer [2006, 2009]) and shock wave experiments (symbols, Brygoo et al. [2015]). The curve represent various initial densities in the experiment.

3.2. Experiments and Simulations of Dense Helium

Helium has also been studied with first-principles computer simulations and high-pressure experiments, although to a lesser extent than hydrogen and deuterium. Early-on diamond anvil cells (DAC) have been used to explore the solid phases of helium and its melting curve. Loubeyre et al. [1982] and Vos et al. [1990] measured the melting temperature of helium 4 from 7.4 to 250 kbar and found it to increase from 50 to 480 K over this pressure interval. Vos et al. [1990] fit the melting line with a simple power law,

$$T_{\text{melt}} = 14.0090 P^{0.6390}, \quad (5)$$

with the pressure P in kbar and the melting temperature in Kelvin. There seems to be some slight deviations from this expression at higher pressure [Datchi et al., 2000] but when extrapolated to the Mbar pressures, this expression is in good agreement with *ab initio* estimates of the melting line [Lorenzen et al., 2009]. Loubeyre et al. [1982] also observed a triple point at 299 K and 116.5 kbar between the liquid and possibly an fcc and an hcp solid phase.

The fluid phase of helium has been studied with shock wave experiments [Nellis *et al.*, 1984]. In the experiments by Eggert *et al.* [2008], that reached 2 Mbar, diamond cells were used to increase the initial density of the helium samples. Because of the complexity and the short time scale of these experiments, the particle velocity, U_p , was not measured directly. Instead of using Eq. 2, the pressures had to be inferred with an impedance matching construction [Brygoo *et al.*, 2015] that relied on a reference material with known properties. For the helium and hydrogen measurements, quartz was used as a reference. After the experimental results had been published, the quartz shock standard was revised [Knudson and Desjarlais, 2009, 2013] and Brygoo *et al.* [2015] reinterpreted the existing hydrogen and helium measurements. The updated helium results are compared to predictions from *ab initio* simulations in Fig. 6.

The EOS of the fluid helium has been characterized by analytical free energy models by Saumon *et al.* [1995] and slightly improved by more complete calculations by Winisdoerffer and Chabrier [2005]. More recently, extensive first-principles simulations have been performed using PIMC for temperatures above 10^3 K and DFT-MD for the lower temperatures [Militzer, 2006, 2009]. The pre-compressed Hugoniot curves predicted by the *ab initio* calculations are displayed in Fig. 6. Overall, there is a good agreement with experimental results but for small initial densities, the measurements predict a slightly higher final shock densities than the DFT-MD simulations.

Unlike hydrogen, helium does not exhibit a molecular phase but one still expects it to become a metal at high pressure. This phenomenon has been investigated with *ab initio* simulations, both by studying the band gap and by computing conductivities and reflectivities. The latter quantity can directly measured during shock experiments. In the solid phase at 0 K, Khairallah and Militzer [2008] showed band gap closure occurs at 21.3 g/cm^3 , or 257 Mbar, using quantum Monte Carlo calculation that are in very good agreement with predictions from GW density functional theory (GW-DFT). Later calculations with electron-phonon coupling by Monserrat *et al.* [2014] suggested that the metallization of helium occurs at even higher pressures. Thus, the metallization pressure of solid helium is at least one order of magnitude higher than that of hydrogen, which is expected to metalize at several Mbar.

The temperature effects on the metallization conditions of fluid helium were studied by Kowalski *et al.* [2007] with DFT and GW methods. They showed that the width of the gap depends on the temperature and estimated a metallization density of 10 g/cm^3 , which was in agreement with calculations in the chemical picture by Winisdoerffer and Chabrier [2005].

The first shock wave experiments that measured the reflectivity of dense helium (1.5 g/cm^3) were reported by Celliers *et al.* [2010]. The size of gap was estimated and gap closure was predicted to occur at a density of 1.9 g/cm^3 . A re-analysis of the experimental data by Soubiran *et al.* [2012], including the temperature effects on the helium gap, showed that experimental findings would also be in agreement with a much higher metallization density of 10 g/cm^3 or above. This implies that unlike hydrogen, pure helium would remain in an atomic and insulating phase over the entire range of pressure-temperature conditions in the interior of giant planets.

4. Hydrogen-Helium Mixtures

4.1. Experiments at Lower Pressure

Because of their significance for planetary science, the hydrogen-helium mixtures have been investigated with various experimental high-pressure techniques. The phase-separation transition in the fluid phase was first studied with static anvil cell experiments with an optical observation of the phase transition. Streett [1973] and Schouten

et al. [1985] reported a partial phase separation into two fluids for pressures up to 50 kbar over a temperature interval from 26 K to nearly room temperature. Loubeyre *et al.* [1985, 1987] used the displacement of the hydrogen Q_1 mode in the Raman spectrum due to the presence of helium to determine the mixing phase diagram up to 100 kbar and 373 K. A detailed phase diagram based on the available experimental data is given in Fig. 9 of Loubeyre *et al.* [1987].

The immiscibility of hydrogen and helium depends on temperature, pressure, and the concentration. For low helium concentration, the demixing is mostly related to the crystallization of hydrogen. For a slightly higher helium concentrations, a triple point is observed for temperatures between 100 and 373 K as the helium concentration is increased from 0.11 to 0.32. This triple point is an equilibrium between a hydrogen-rich solid phase and two liquid phases of intermediate and high helium concentrations.

Loubeyre *et al.* [1987] also defined a critical point that, for a given temperature, marks the minimum pressure for any mixtures to show phase separation. For instance, at 295 K, the critical point is at 51 kbar, while the triple point is at 62 kbar (see Fig. 9 of Loubeyre *et al.* [1987]). While these results represent the best laboratory measurements of hydrogen-helium mixtures to date, their relevance for the extreme pressure and temperature conditions in giant planet interiors remains to be determined.

4.2. Simulations of Hydrogen-Helium Phase Separation

Because of the relevance to giant planet interiors, hydrogen-helium mixtures have been the subject of various first-principles studies. Early DFT simulations by Klepeis *et al.* [1991] and Pfaffenzeller *et al.* [1995] focused on ground state calculations of solid hydrogen-helium mixtures because DFT-MD simulation at high temperature could not yet been performed efficiently. Homogeneous hydrogen-helium mixtures were also studied with path integral Monte Carlo simulations [Militzer, 2005] but it has proved challenging to apply this method below 10 000 K where one expects phase separation in the fluid.

Once more computer time became available, Vorberger *et al.* [2007] studied nonlinear mixing effects in hydrogen-helium mixtures with DFT-MD simulations. It was demonstrated that, for a given pressure and temperature, the presence of helium stabilizes the hydrogen molecules and shifts the molecular-to-metallic transition in hydrogen to higher

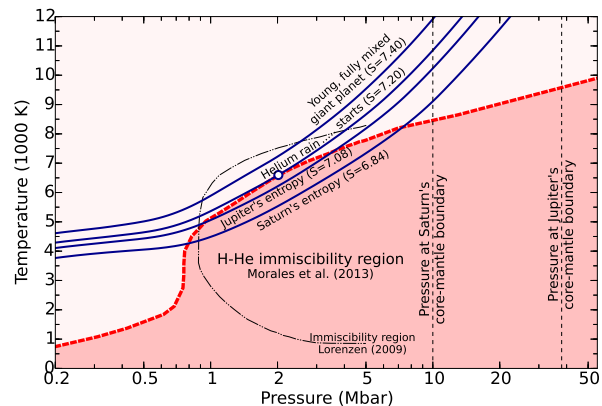


Figure 7. Hydrogen-helium miscibility diagram. The solid lines show DFT-MD adiabat from Militzer and Hubbard [2013] labeled with their entropy in units of k_B per electron. The shaded area is the immiscibility region calculated by Morales *et al.* [2013] that we extrapolated towards higher pressures.

pressures. A direct demonstration of the phase separation with first-principles method was still missing, however. This problem was elegantly solved with the Gibbs free energy calculations by [Morales *et al.*, 2009, 2013] who determined the full nonideal entropy of mixing with DFT-MD simulations. The emerging immiscibility region is shown in Fig. 7 and was used in Jupiter interior model by Hubbard and Militzer [2016].

Lorenzen *et al.* [2009] also performed DFT-MD simulations to derive the immiscibility region in hydrogen-helium mixtures. While non-ideal mixing effects of pressure and internal energy were included in the calculation, only the ideal entropy of mixing was considered. The resulting immiscibility region, shown in Fig. 7, is surprisingly close to the results by Morales *et al.* [2013]. Still at 2 Mbar, Lorenzen *et al.* [2009] overestimate the immiscibility temperature by 1000 K. Below 3000 K, the Lorenzen *et al.* [2009] calculations become invalid because nonideal contributions to the mixing entropy become very important. Without an explicit calculation, it is difficult to predict how important nonideal mixing effects are. For instance, Soubiran and Militzer [2015] found that dense molecular mixtures of hydrogen and water behaved approximately ideal while Wilson and Militzer [2010] demonstrated that one may obtain the wrong answer in helium rain sequestration calculations unless the nonideal entropy of mixing is included correctly.

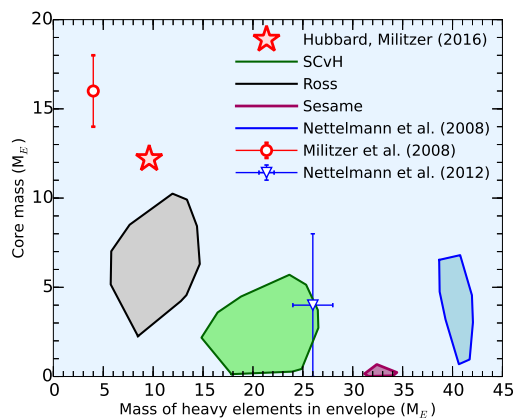


Figure 8. The mass of the dense central core and amount heavy Z elements in the envelope is compared for different models of Jupiter’s interior. Results reported by Saumon and Guillot [2004] were complemented with model predictions by Militzer *et al.* [2008]; Nettelmann *et al.* [2008, 2012]; Hubbard and Militzer [2016].

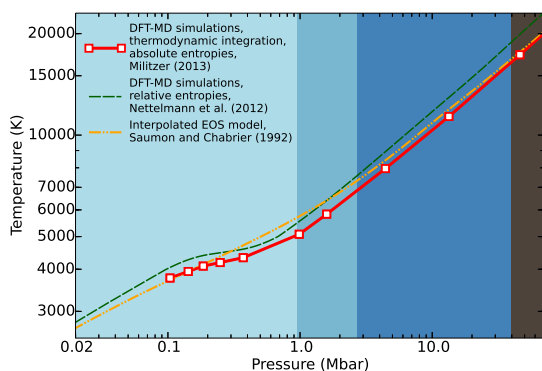


Figure 9. Different theoretical predictions for Jupiter’s interior adiabat. The shaded areas corresponds to the layers in figure 3.

Deep inside the immiscibility region, one can also observe the phase-separation of the hydrogen and helium directly in the DFT-MD simulations [Soubiran *et al.*, 2013; Militzer, 2013], which provides an independent confirmation of the results from Gibbs free energy calculations.

The most common structure assumed for Jupiter’s interior is a three layer model [Guillot *et al.*, 2004; Saumon and Guillot, 2004; Nettelmann *et al.*, 2012; Hubbard and Militzer, 2016] that consists of a dense, heavy element rich, central core, along with a metallic inner envelope and a molecular outer envelope, both comprised predominately of hydrogen and helium. Each layer is assumed to be adiabatic and of constant composition. The entropy, the helium mass fraction, Y , and mass fraction of heavier elements, Z , may differ between the layers. Temperature and pressure are typically assumed to be continuous across layer boundaries.

5. Current Jupiter Interior Models

One key constraint on Jupiter’s atmosphere are the temperature-pressure measurements by the *Galileo* entry probe shown in Fig. 2. This can be used as a starting point for the temperature profile in the outer layer. In addition, the *Galileo* entry probe provided measurements of Y and Z , which are typically taken to be representative of at least the outer envelope composition.

Furthermore, models for Jupiter’s interior are constrained by the total mass of the planet, along with the measured gravitational moments J_2 and J_4 discussed in section 2. To relate given values of J_n to interior structure, the planet is assumed to be in hydrostatic equilibrium in the rotating frame, and a unique barotrope $P = P(\rho)$ is derived from the equation of state to relating the pressure P and the mass density ρ for a given entropy and composition. An acceptable model must then reproduce the external gravity terms within the uncertainty of the observations.

Determining the J_n of a model requires a self-consistent calculation of the planet’s rotation-induced shape and gravitational field. While analytic high-order perturbative theories for the zonal harmonic coefficients have been developed [Zharkov and Trubitsyn, 1978], the high expected precision of the *Juno* model has prompted the development of

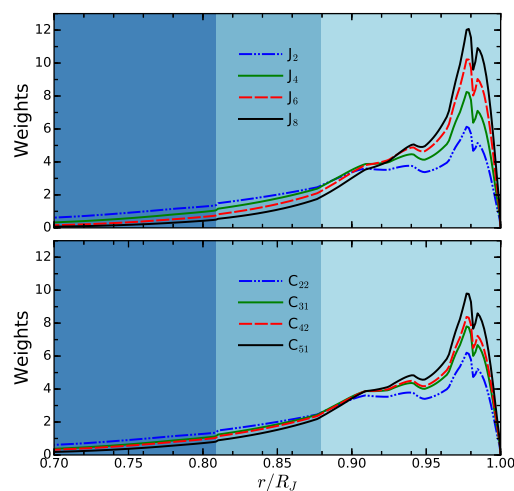


Figure 10. Contribution of spheroids to Jupiter’s external gravitational zonal harmonic coefficients (top) and tesseral coefficients (bottom) as a function of radius. Weights are normalized such that the sum of contributions equals the total number of layers ($N = 511$). The shaded areas corresponds to the layers in figure 3. Tesseral moments of the same order (i.e. C_{31} and C_{33}) have indistinguishable radial distributions.

more precise non-perturbative, numerical methods for calculating J_n [Hubbard, 2013; Wisdom and Hubbard, 2016]. Using this method, Hubbard and Militzer [2016] suggested that the actual J_4 of Jupiter might lie outside of the error bars reported by Jacobson [2003] in order to be consistent with the DFT-MD equation of state by Militzer and Hubbard [2013].

In Fig. 8, we compare the core sizes and amounts of heavy Z elements in the outer layers that were inferred from model calculations that assumed various EOSs of hydrogen-helium mixtures. The large spread of predictions by different equations of state highlights the importance of an accurate equation of state for the interpretation of measurements by *Juno* and future missions. Interior models based on the Sesame [Kerley, 1983], Ross [1998], and Saumon *et al.* [1995] EOSs yield core masses of less than $10 M_{\oplus}$ and would thus be inconsistent with the *core accretion* assumption for the planet's formation [Pollack *et al.*, 1996] unless an initial dense core has been eroded by convection (see section 6.3). However, these EOSs all yield substantial core masses between 10 and $25 M_{\oplus}$ for Saturn's interior [Saugmon and Guillot, 2004]. This means, if core erosion indeed occurred in giant planet interiors, it had to be much stronger in Jupiter's interior than in Saturn. This is not inconceivable since Jupiter is three times heavier and thus more convective energy would be available to lift up heavy materials against forces of gravity.

On the other hand, Jupiter interior models on DFT-MD EOS by Militzer *et al.* [2008] and Hubbard and Militzer [2016] predict a larger central core for Jupiter of $12 M_{\oplus}$ or more. The latter model assumed that helium rain occurred on this planet, which suggests Jupiter's interior may not be too different from that of Saturn. The DFT-MD based models by Nettelmann *et al.* [2008, 2012] predict a very small central core of $8 M_{\oplus}$ or less, which requires further discussion.

Figure 9 shows that the adiabats are very different. Militzer and Hubbard [2013] computed absolute entropies. Each point in Fig. 9 was determined with an independent calculation with the *ab initio* thermodynamic integration (TDI) method [de Wijs *et al.*, 1998; Alfè *et al.*, 2000; Morales *et al.*, 2009; Wilson and Militzer, 2010]. The fact that a smooth curve emerges demonstrates that the statistical error bars can be controlled very well with TDI approach [Militzer, 2013]. The computed *ab initio* entropies also agree well with the Saumon *et al.* [1995] EOS model in the limit of low and high pressure where one expects this semi-analytical model to work well since it was designed to reproduce the EOS of a weakly interacting molecular gas at low pressures and a two-component plasma in the high-pressure limit. For intermediate pressures from 0.2 to 20 Mbar, figure 9 shows deviations between the *ab initio* TDI approach [Militzer, 2013] and Saumon *et al.* [1995] EOS model because little information about the properties of hydrogen near the molecular-to-metallic transition was available when this model was constructed. Furthermore, the deviations are seen in a region where Saumon *et al.* [1995] interpolated between their descriptions for molecular and metallic hydrogen. Deviations in this regions are, thus, not unexpected.

It is unusual, however, that the adiabats DFT-MD by Nettelmann *et al.* [2012] are significantly higher in temperature than those by Militzer and Hubbard [2013].

There are three main reasons for the deviations in the *ab initio* adiabats in Fig. 8 that need to be considered. (1) Since Nettelmann *et al.* [2012] did not use the TDI technique, absolute entropies could not be determined. Instead the slope of the adiabat was inferred from the pressure and internal energies that are accessible with standard *ab initio* simulations. In addition to the slope, an anchor point at ~ 0.1 Mbar is needed to start the computation of the adiabat. Already at this low pressure, the Nettelmann *et al.* [2012] adiabat is significantly higher than that reported by Militzer and Hubbard [2013]. If the anchor point in the Nettelmann *et al.* [2012] calculation is chosen differently, the

agreement of the adiabats improves substantially (see Fig. 11 in Militzer and Hubbard [2013]).

(2) When the slopes of the adiabats are determined from the *ab initio* pressures and internal energy, $(\partial T/\partial V)_S = -T(\partial P/\partial T)_V / (\partial E/\partial T)_V$ [Militzer, 2009], one needs P and E on a fine grid of density-temperature points for interpolation. In practice, one can only perform a finite number of simulations and the results have statistical uncertainties.

(3) Finally, Nettelmann *et al.* [2012] computed the EOS for hydrogen and helium separately and then invoked linear mixing approximation to characterize the H-He mixture while Militzer and Hubbard [2013] performed fully interacting simulations on one representative H-He mixture with mixing ratio ($Y=0.245$) and then used the linear mixing approximation only to perturb around this concentration. However, far outside of the H-He immiscibility region one expects the linear mixing approximation to be reasonable.

We gathered that the last two points are of lesser importance and concluded that the main reason for the deviations in Fig. 8 was the choice to take an anchor point from the analytical fluid variational theory [Nettelmann *et al.*, 2012].

The temperature profile is important for models of giant planet interiors. For a given pressure, a higher temperature implies a lower density, which is compensated by a higher fraction of heavy Z elements when Jupiter interior models are constructed with the goal of matching the measured values of the planet's gravity field. A higher-than-solar heavy element fraction would imply that the process, that led to Jupiter's formation, was more efficient in capturing dust and ice than gas. Therefore the characterization of H-He adiabats with theoretical and experimental techniques is important to understand Jupiter's formation. At the same time, the interaction of heavy Z elements with dense H-He mixtures needs to be characterized. Soubiran and Militzer [2016] performed simulations for a variety of heavy elements. This is the first study to investigate the properties of multi-component mixtures of H, He and heavy elements. It shows that the heavy elements slightly influence the density profile of giant planets. Fig. 4 shows one representative snapshot from a ternary hydrogen-helium-iron mixture.

Giant planet interior models often invoke a different chemical composition for molecular and metallic layers. The original justification for introducing this additional degree of freedom was a first order phase transition between molecular and metallic hydrogen. This argument is not supported by DFT-MD simulations that show a smooth transition of properties with increasing P Vorberger *et al.* [2007]; Militzer *et al.* [2008]. More recently it has been proposed that the separation between layers in Jupiter corresponds to a narrow region of helium immiscibility [Guillot *et al.*, 2004; Hubbard and Militzer, 2016]. A schematic depiction of this model is shown in Figure 3. The precipitation of helium through this layer is expected to lead to an intrinsic density difference that may inhibit effective convection between the inner and outer envelope. This may allow Jupiter's deep interior to be hotter than would be expected for a single layer convection envelope. Hubbard and Militzer [2016] identify this region by identifying the pressures where the present-day adiabat for the outer envelope intersects H-He immiscibility region from Morales *et al.* [2013] (Figure 2). This leads to a prediction of a present-day helium rain region between $\sim 0.81 - 0.88a$. This model has an important evolutionary distinction, since the planet's temperature profile would have initially been above the immiscibility region, meaning the envelope is initially homogeneous, with the demixing layer forming and growing as the planet cools.

Figure 10 shows the contribution functions for zonal and tesseral harmonics of degree 2, 4, 6, and 8. As suggested by Eq. 1, these functions are progressively more peaked toward the surface with increasing degree. There is no significant

direct contribution from the central region where a central core might exist. Moreover, the contribution functions overlap substantially, implying that values of the harmonics for a given density distribution are strongly correlated. The mass of a dense central core cannot be inferred solely from a finite set of harmonic coefficients; instead it must emerge from a simultaneous fit to all available constraints on interior structure. This process is strongly dependent on the precision of the thermodynamic model used to construct the barotrope.

6. Discussion of Jupiter Models

6.1. The Adiabatic Assumption

The modeling of a giant planet's thermal structure rely on a few simple equations once spherical symmetry is assumed. The first arises from the conservation of mass,

$$\frac{dm}{dr} = 4\pi r^2 \rho, \quad (6)$$

where m is the mass enclosed in a sphere of radius r and ρ the local density. Second, one assumes hydrostatic equilibrium, which is a reasonable assumption as no shocks or other dynamical effects of any significance are present. This provides a constraint on the pressure profile:

$$\frac{dP}{dr} = -\frac{Gm\rho}{r^2}, \quad (7)$$

where P is the local pressure and G is the gravitational constant. In the simplest case, just one additional relationship is required to determine the interior structure of a planet, which is the equation of state, $\rho = \rho(P, T)$, of the material in each layer. This require one to introduce additional assumptions for the temperature profile unless the pressure is dominated by contributions from a degenerate electron gas. In general the temperature profile, $T(r)$, is set by the processes that transfer thermal energy throughout the planet. The relationship of the temperature and pressure profiles can be expressed in the following convenient form,

$$\frac{dT}{dr} = \frac{T}{P} \frac{dP}{dr} \nabla(T, P), \quad (8)$$

with the temperature gradient $\nabla(T, P) \equiv \frac{d \ln T}{d \ln P}$, which is set by the energy transfer mechanisms. In the interiors of

planets and stars, there are three possible mechanisms of energy transfer: radiation, convection, and conduction. To first approximation, the process that leads to smallest temperature gradient will be the most efficient one and therefore dominate the energy transfer in a particular layer.

$$\nabla(T, P) = \min(\nabla_{\text{ad}}, \nabla_{\text{rad}}, \nabla_{\text{cond}}). \quad (9)$$

The adiabatic gradient, ∇_{ad} , corresponds to the temperature gradient that arises in a convecting material. It is determined by making the assumption that an advected parcel of fluid rises fast enough to prevent energy loss through diffusion or radiation to the surrounding fluid. We also assume that the evolution is slow enough for the pressure inside and outside of the parcel to reach an equilibrium. In this case the transformation is quasi-static and thus isentropic. The resulting adiabatic gradient directly follows from the equation of state,

$$\nabla_{\text{ad}} = \left. \frac{\partial \ln T}{\partial \ln P} \right|_s. \quad (10)$$

In the case of a purely conductive layer, the thermal conductivity, λ , is the key quantity. From Fourier's law, we know that the heat flux through the sphere of radius r is given by $F(r) = -\lambda \frac{dT}{dr}$. The heat flux is related to the luminosity, l , by $F(r) = \frac{l(r)}{4\pi r^2}$. From these relations and Eq. 7, we find,

$$\nabla_{\text{cond}} = \frac{lP}{4\pi\lambda T Gm\rho}. \quad (11)$$

In case of a purely radiative layer, under the diffusive approximation, we find that the radiative gradient is given by [Rutten, 2003]:

$$\nabla_{\text{rad}} = \frac{3\kappa lP}{64\pi\sigma T^4 Gm}, \quad (12)$$

with κ the opacity of the material and σ the Stefan-Boltzmann constant.

We can perform an order-of-magnitude calculation to determine which energy transfer mechanism dominates in different layers of a giant planet. Radiation is only important in the upper most atmosphere because the radiative opacity is high in all deeper layers. For instance in the metallic region in the deep interiors of giant planets, free electrons absorb photons very efficiently. In Fig. 11, we compare the conductive and adiabatic gradients for the interior of a giant planet. The adiabatic gradient was derived from the equation of state by Saumon *et al.* [1995]. For this comparison, one can assume that the luminosity is constant throughout the envelope [Mordasini *et al.*, 2012] and use the value of $8.7 \times 10^{-10} L_{\odot}$.

An approximate value for thermal conductivity can be derived from the fully ionized model of Potekhin *et al.* [2015], which an upper limit for the conductivity because not all electrons are fully ionized and scattering processes matter in dense hydrogen-helium mixtures. Fig. 11 underlines that the adiabatic gradient is nearly two orders of magnitude lower than the conductive gradient which indicates that the convection is the most efficient mechanism and that the isentropic approximation is valid as long as the envelope has a homogeneous composition.

6.2. Over-turning and Double-Diffusive Convection

The adiabatic assumption relies on the hypothesis that the envelope is entirely and efficiently convective. However, as Stevenson [Stevenson, 1985] pointed out more than three decades ago, the interior of a giant planet may not be homogeneous in composition for a number of reasons including

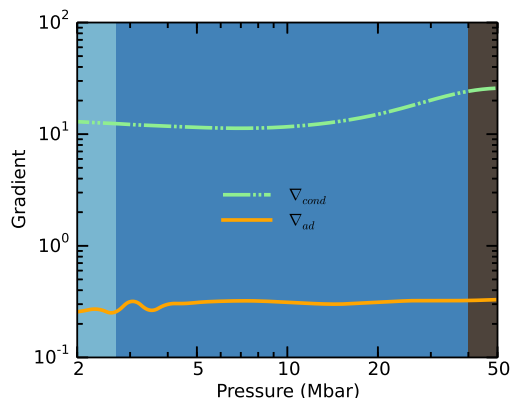


Figure 11. Adiabatic and conductive gradients along a Jupiter-type profile. The model and the adiabatic gradient are computed with the SCvH EOS [Saumon *et al.*, 1995]. The thermal conductivity is estimated with the fully ionized model [Potekhin *et al.*, 2015]. The shaded areas corresponds to the layers in figure 3.

late planetesimal accretion, core erosion and phase separation. In this case, even if the thermal density gradient is destabilizing, an intrinsic density gradient of composition can become stabilizing if there is an excess of heavy materials in the warm regions and lighter materials in the cold regions. This process is termed double-diffusive convection or semi-convection in the literature. To characterize the behavior of the fluid in the presence of a gradient of temperature $\nabla_T = \frac{d \ln T}{d \ln P}$ and a gradient of mean molecular weight (equivalent to a gradient of composition) $\nabla_\mu = \frac{d \ln \mu}{d \ln P}$, we define a density ratio [Stern, 1960; Leconte and Chabrier, 2012]:

$$R_\rho = \frac{\alpha_T}{\alpha_\mu} \frac{\nabla_T - \nabla_{\text{ad}}}{\nabla_\mu}, \quad (13)$$

with $\alpha_T = -\left. \frac{\partial \ln \rho}{\partial \ln T} \right|_{P, \mu}$ and $\alpha_\mu = \left. \frac{\partial \ln \rho}{\partial \ln \mu} \right|_{P, T}$. In the case of a destabilizing temperature gradient, $\nabla_T - \nabla_{\text{ad}} > 0$, but a stabilizing compositional gradient, $\nabla_\mu > 0$, the convective instability criterion then becomes $R_\rho^{-1} < 1$, called the Ledoux criterion [Ledoux, 1947]. However, this is not a simple stability criterion and there are three different observed behaviors (see Fig. 1 in Leconte and Chabrier [2012] for a schematic diagram).

The stability criterion is given by

$$R_\rho^{-1} > \frac{Pr + 1}{Pr + \tau}, \quad (14)$$

with $Pr = \frac{\nu}{\kappa_T}$, the Prandtl number, which is the ratio between the kinematic viscosity and the thermal diffusivity, and $\tau = \frac{D}{\kappa_T}$, the ratio of the solute particle diffusivity and the thermal diffusivity. If this criterion is verified then the layer is stably stratified and no dynamics is expected.

In the case of a marginally stable system,

$$R_{\min}^{-1} < R_\rho^{-1} \leq \frac{Pr + 1}{Pr + \tau}, \quad (15)$$

a system of oscillatory convection, also called turbulent diffusion, can occur.

The last case is the layered convection where well-defined layers develop with a small-scale convection, when

$$1 < R_\rho^{-1} \leq R_{\min}^{-1}. \quad (16)$$

The critical value of R_{\min}^{-1} depends on the properties of the fluid under study and its exact value is difficult to estimate [Radko, 2003; Rosenblum et al., 2011; Mirouh et al., 2012].

While the oscillatory convection seems irreconcilable with the observed heat flux of Jupiter or Saturn [Leconte and Chabrier, 2013; Nettelmann et al., 2015], layered convection could explain the observed properties of the planets. In this layered convection, the envelope is divided in successive layers alternating between convective sub-cells and diffusive layers of height h_c and h_d respectively. In a steady state, the typical timescale for the diffusive and the convective layers have to be similar leading to a height ratio:

$$\frac{h_d}{h_c} = Ra_\star^{-1/4}, \quad (17)$$

where Ra_\star is the modified Rayleigh number defined as [Leconte and Chabrier, 2012; Spruit, 2013]:

$$Ra_\star = \frac{\alpha_T g H_P^3}{\kappa_T^2} \alpha^4 (\nabla_T - \nabla_{\text{ad}}), \quad (18)$$

with g the local gravitational acceleration, H_P the pressure scale height and $\alpha = h_c/H_P$. It is interesting to note in Eq. (17), that the heights ratio is proportional to $\kappa_T^{1/2}$.

Yet, there is a significant difference when one uses the fully ionized model [Potekhin et al., 2015] or the *ab initio* calculations [French et al., 2012] to estimate the thermal diffusivity, leading to significant uncertainty in the height ratio. Secondly, Eq. (18) shows that α is a key parameter yet unconstrained *a priori*.

Leconte and Chabrier [2012] explored the possible giant planet structures when layered convection is assumed. If we consider a fixed α throughout the envelope, it is possible to build models that match all the observable properties of Jupiter and Saturn, including the heat flux and the gravitational moments. The permitted values for α for Jupiter range from 3×10^{-5} to 10^{-2} which gives a number of layers ranging between 100 and 3×10^4 . For a higher number of layers, the interior becomes too hot and the average density too low. A very interesting outcome of the layered convection assumption is that the total content of heavy element increases from $40 M_\oplus$ in the adiabatic case to $63 M_\oplus$ for the most extreme layered convection considered, out of which only 0-0.5 M_\oplus is in a dense central core. Moreover, as the layered convection is less efficient than large-scale convection in transporting heat, they suggested it as a possible explanation of the excess luminosity of Saturn [Leconte and Chabrier, 2013].

Leconte and Chabrier [2012] did not make any assumption on the origin of the initial gradient of composition for their layered convection model, but one possible origin is the phase separation of hydrogen and helium [Christensen and Yuen, 1985]. When considering a layered or double-diffusive convection, the fluxes of heat and of composition must be carefully characterized since they affect the evolution of the planet's interior. To better constrain the evolution of Jupiter in the case of a H-He phase separation, Nettelmann et al. [2015] used numerical results of layered and double-diffusive convection simulations with scaling laws for the heat flux [Mirouh et al., 2012; Wood et al., 2013]. However, these scaling laws were computed for the case of miscible fluids and do not consider the possible influence the phase separation may have on the fluxes. Nettelmann et al. [2015] based their model on thermodynamic properties coming from the SCvH EOS [Saumon et al., 1995] and on the phase diagram computations of Lorenzen et al. [2009, 2011]. They observed that to match the Galileo probe measured helium abundance they needed to modify the shape of the phase diagram, or the outer layer would become too depleted in helium. They also found that Jupiter's cooling age was too long by 1.1 Gyr with He rain and the adiabatic assumption (their Figure 16). In the case of a layered convection, they found possible models that would match the observations and the age of Jupiter with layers of 100 to 1000 m height.

While important advances have been made using non-adiabatic models, they have also raised many questions that need to be addressed to understand the formation of layered convection state. First, the H-He phase diagram must be better constrained. Likewise, the heat and particle fluxes must be better constrained along with the influence of the phase separation and corresponding release of latent heat. Last, the length scale of the convective cells is likely to evolve in time with merging mechanisms [Spruit, 2013] that will be competing with the phase separation. The dynamical effects of these different phenomena could have an important impact on the predicted evolution of the giant planets.

6.3. Core Erosion

The existence and size of a dense central core of Jupiter is an outstanding question. Although a dense central core is a natural outcome of the preferred *core accretion* hypothesis

for Jupiter's formation [Mizuno *et al.*, 1978; Bodenheimer and Pollack, 1986; Pollack *et al.*, 1996], it would not necessarily result in a planet formed by the collapse region of the disk under self-gravity, e.g. [Boss, 1997]. Moreover, it has been suggested by Stevenson [1982], that at high pressures the stable phases of the high-density materials may become soluble in liquid hydrogen. As a result, an initial dense core with rocky or icy composition might erode, with the dense material being redistributed over a larger region of the planet. This is one mean of forming a density gradient necessary for a double diffusive region in the planet's interior [Chabrier and Baraffe, 2007; Leconte and Chabrier, 2012; Mirouh *et al.*, 2012]. While many interior models (e.g. [Hubbard and Militzer, 2016]) require a dense central core of up to ~ 20 Earth masses to match the observed gravitational moments, the model predictions are not sensitive to the radius, or equivalently density, of this core. Various core compositions are plausible. It could be a terrestrial iron-rock mixture, a iron-rock-ice mixture, or be a more diffuse mixture of heavy elements with liquid hydrogen and helium.

The solubility of various materials have been assessed with DFT-MD calculations comparing Gibbs free energy of the solution compared to the separated materials. This is accomplished by performing DFT-MD simulations with a two-step thermodynamic integration method [Morales *et al.*, 2009; Wilson and Militzer, 2010]. A number of studies used this to find the solubility of various analogue planetary materials in liquid metallic hydrogen. Dissolution was found to be strongly favorable for both water [Wilson and Militzer, 2012a] and iron [Wahl *et al.*, 2013] in the cores of Jupiter and Saturn. Solubility of rocky analogues MgO [Wilson and Militzer, 2012b] and SiO₂ [Gonzalez-Cataldo *et al.*, 2014] are more moderate, but are still predicted to dissolve in Jupiter's interior. The high-pressure solubility of all these materials with metallic hydrogen is consistent with their increasing metallic nature at high pressures. Thus a dense central core of Jupiter is expected to be presently eroded or eroding. However, the redistribution of heavy elements by inefficient double-diffusive convection may be slow compared to evolutionary timescales [Chabrier and Baraffe, 2007], keeping most of the heavy elements confined to a relatively small region in the planet's deep interior.

7. Conclusions

Despite the obvious difficulties to predict how the fields of planetary science and high-pressure physics will develop in the coming 25 years, a few statements can be made. After Juno, we expect further space missions to visit all four giant planets in our solar system. Since Uranus and Neptune have not been studied as often as Jupiter and Saturn, we expect to gather fundamental knowledge about the history of outer solar system from future ice giant missions. It would be worthwhile to include entry probes since they provide so much more detailed information about the atmospheric composition than remote observations can.

We also expect first-principles computer simulations to become more accurate. Standard DFT-MD methods may be replaced with quantum Monte Carlo methods.

As far as high-pressure laboratory experiments are concerned, a direct measurements of hydrogen-helium phase separation would be of significant importance for our understanding of gas giant interiors. We also anticipate that cold, metallic hydrogen will be produced in static compression experiments at room temperature.

Acknowledgments

The authors knowledge support from the U.S. National Science Foundation, from the NASA mission Juno and a Cassini data analysis grant. T. Guillot provided valuable

comments on Fig. 2. The data in the figures can be obtained from the references or by contacting the first author.

References

- Alfè, D., M. J. Gillan, and G. D. Price (2000), *Nature*, *405*, 172.
- Belov, S., G. Boriskov, A. Bykov, R. Il'kaev, N. Luk'yanov, A. Matveev, O. Mikhailova, V. Selemir, G. Simakov, R. Trunin, I. Trusov, V. Urlyn, V. Fortov, and A. Shuikin (2002), *JETP Lett.*, *76*, 443.
- Benedict, L. X., K. P. Driver, S. Hamel, B. Militzer, T. Qi, A. A. Correa, A. Saul, and E. Schwegler (2014), A multiphase equation of state for carbon addressing high pressures and temperatures, *Phys. Rev. B*, *89*, 224,109.
- Beule, D., W. Ebeling, and A. Förster (1999), *Phys. Rev. B*, *59*, 14,177.
- Bodenheimer, P., and J. B. Pollack (1986), Calculations of the accretion and evolution of giant planets: The effects of solid cores, *Icarus*, *67*(3), 391–408, doi:10.1016/0019-1035(86)90122-3.
- Bonev, S. A., B. Militzer, and G. Galli (2004), *Phys. Rev. B*, *69*, 014,101.
- Boriskov, G. V. *et al.* (2003), *Dokl. Phys.*, *48*, 553.
- Boss, A. P. (1997), Giant Planet Formation by Gravitational Instability, *Science* (80-.), *276*(5320), 1836–1839, doi:10.1126/science.276.5320.1836.
- Brygoo, S., M. Millot, P. Loubeyre, A. E. Lazicki, S. Hamel, T. Qi, P. M. Celliers, F. Coppari, J. H. Eggert, D. E. Fratantuono, D. G. Hicks, J. R. Rygg, R. F. Smith, D. C. Swift, G. W. Collins, and R. Jeanloz (2015), Analysis of laser shock experiments on precompressed samples using a quartz reference and application to warm dense hydrogen and helium, *J. Appl. Phys.*, *118*, 195,901, doi:10.1063/1.4935295.
- Bunker, A., S. Nagel, R. Redmer, and G. Röpkke (1997), *Phys. Rev. B*, *56*, 3094.
- Campbell, J. K., and S. P. Synnott (1985), *Astron. J.*, *90*, 364.
- Celliers, P. M., P. Loubeyre, J. H. Eggert, S. Brygoo, R. S. McWilliams, D. G. Hicks, T. R. Boehly, R. Jeanloz, and G. W. Collins (2010), *Phys. Rev. Lett.*, *104*, 184,503.
- Chabrier, G., and I. Baraffe (2007), Heat Transport in Giant (Exo)planets: A New Perspective, *Astrophys. J.*, *661*(1), L81–L84, doi:10.1086/518473.
- Christensen, U. R., and D. a. Yuen (1985), Layered Convection Induced by Phase Transitions, *J. Geophys. Res.*, *90*(B12), 10,291.
- Collins, G. W., L. B. D. Silva, P. Celliers, D. M. Gold, M. E. Foord, R. J. Wallace, A. Ng, S. V. Weber, K. S. Budil, and R. Cauble (1998), *Science*, *281*, 1178.
- Da Silva, I. B., P. Celliers, G. W. Collins, K. S. Budil, N. C. Holmes, W. T. J. Barbee, B. A. Hammel, J. D. Kilkenny, R. J. Wallace, M. Ross, R. Cauble, A. Ng, and G. Chiu (1997), *Phys. Rev. Lett.*, *78*, 483.
- Datchi, F., P. Loubeyre, and R. Le Toullec (2000), Extended and accurate determination of the melting curves of argon , helium , ice H 2 O . . . , and hydrogen H 2 . . . , *Phys Rev B*, *61*(10), 6535.
- de Wijs, G. A., G. Kresse, and M. J. Gillan (1998), *Phys. Rev. B*, *57*, 8223.
- Driver, K. P., and B. Militzer (2012), *Phys. Rev. Lett.*, *108*, 115,502.
- Driver, K. P., and B. Militzer (2015), First-principles simulations and shock Hugoniot calculations of warm dense neon, *Phys. Rev. B*, *91*, 045,103.
- Driver, K. P., and B. Militzer (2016), *Phys. Rev. B*, *93*, 064,101.
- Driver, K. P., F. Soubiran, S. Zhang, and B. Militzer (2015), *J. Chem. Phys.*, *143*, 164,507.
- Ebeling, W., and W. Richert (1985a), *Phys. Lett. A*, *108*, 85.
- Ebeling, W., and W. Richert (1985b), *Phys. Stat. Sol.*, *128*, 467.
- Ebeling, W., and R. Sändig (1973), *Ann. Phys.*, *28*, 289.
- Ebeling, W., A. Förster, W. E. Fortov, V. K. Gryanzov, and A. Y. Polishchuk (1991), B. G. Teubner Verlagsgesellschaft, Stuttgart, Leipzig.

- Eggert, J., S. Brygoo, P. Loubeyre, R. S. McWilliams, P. M. Celliers, D. G. Hicks, T. R. Boehly, R. Jeanloz, and G. W. Collins (2008), Hugoniot data for helium in the ionization regime, *Phys. Rev. Lett.*, *100*(March), 124,503, doi:10.1103/PhysRevLett.100.124503.
- Fortov, V. E., R. I. Ilkaev, V. A. Arinin, V. V. Burtzev, V. A. Golubev, I. L. Iosilevskiy, V. V. Khrustalev, A. L. Mikhailov, M. A. Mochalov, V. Y. Ternovoi, and M. V. Zhernokletov (2007), *Phys. Rev. Lett.*, *99*, 185,001.
- Fowler, R., and E. Guggenheim (1965), Cambridge University Press, Cambridge, UK.
- French, M., A. Becker, W. Lorenzen, N. Nettelmann, M. Bethkenhagen, J. Wicht, and R. Redmer (2012), Ab Initio Simulations for Material Properties Along the Jupiter Adiabatic, *Astrophys. J. Suppl. Ser.*, *202*(2011), 5, doi:10.1088/0067-0049/202/1/5.
- Galileo (), Galileo probe archive, <http://pds-atmospheres.nmsu.edu/cgi-bin/getdir.pl?volume=gp-0001>, accessed: 2016-07-21.
- Gonzalez-Cataldo, F., H. F. Wilson, and B. Militzer (2014), *Astrophys. J.*, *787*, 79.
- Guillot, T., D. J. Stevenson, W. B. Hubbard, and D. Saumon (2004), The interior of Jupiter, In: *Jupiter. The planet*, p. 35.
- Hubbard, W. B. (2013), Concentric Maclaurin Spheroid Models of Rotating Liquid Planets, *Astrophys. J.*, *768*(1), 43, doi:10.1088/0004-637X/768/1/43.
- Hubbard, W. B., and B. Militzer (2016), *Astrophys. J.*, *820*, 80.
- Hugoniot, H. (1887), Mémoire sur la propagation des mouvements dans les corps et spécialement dans les gaz parfaits (première partie), *Journal de l'École Polytechnique*, *57*, 3.
- Hugoniot, H. (1889), Mémoire sur la propagation des mouvements dans les corps et spécialement dans les gaz parfaits (deuxième partie), *Journal de l'École Polytechnique*, *58*, 1.
- Jacobson, R. (2001), The Gravity Field of the Jovian System and the Orbits of the Regular Jovian Satellites, in *AAS/Division Planet. Sci. Meet. Abstr. #33, Bulletin of the American Astronomical Society*, vol. 33, p. 1039.
- Jacobson, R. A. (2003), JUP 230 Orbital Solution.
- Jacobson, R. A. (2013), JUP310 Orbit Solution.
- Janssen, M. A., S. T. Brown, J. E. Oswald, and A. Kitiyakara (2014), Juno at Jupiter: The Juno microwave radiometer (MWR), *2014 39th International Conference on Infrared, Millimeter, and Terahertz waves (IRMMW-THz), F2/D-39.1*.
- Juranek, H., and R. Redmer (2000), *J. Chem. Phys.*, *112*, 3780.
- Kaspi, Y., and E. Galanti (2016), An adjoint-based method for the inversion of the Juno and Cassini gravity measurements into wind fields, *Astrophys. J.*, *820*, 91.
- Kerley, G. I. (1983), p. 107, American Chemical Society, Washington DC.
- Khairallah, S. A., and B. Militzer (2008), First-Principles Studies of the Metallization and the Equation of State of Solid Helium, *Phys Rev Lett*, *101*, 106,407, doi:10.1103/PhysRevLett.101.106407.
- Kitamura, H., and S. Ichimaru (1998), *J. Phys. Soc. Japan*, *67*(3), 950.
- Klepeis, J. E., K. J. Schafer, T. W. B. III, and M. Ross (1991), *Science*, *254*, 986.
- Knudson, M. D., and M. P. Desjarlais (2009), *Phys. Rev. Lett.*, *103*, 225,501.
- Knudson, M. D., and M. P. Desjarlais (2013), *Phys. Rev. B*, *88*, 184,107.
- Knudson, M. D., D. L. Hanson, J. E. Bailey, C. A. Hall, J. R. Asay, and W. W. Anderson (2001), *Phys. Rev. Lett.*, *87*, 225,501.
- Knudson, M. D., M. P. Desjarlais, A. Becker, R. W. Lemke, K. R. Cochran, M. E. Savage, D. E. Bliss, T. R. Mattsson, and R. Redmer (2015), *Science*, *348*, 1455.
- Kowalski, P. M., S. Mazevet, D. Saumon, and M. Challacombe (2007), Equation of state and optical properties of warm dense helium, *Phys Rev B*, *76*, 075,112, doi:10.1103/PhysRevB.76.075112.
- Landau, L., and Y. Zeldovich (1943), *Acta Physico-Chem. URSS*, *18*, 1943.
- Leconte, J., and G. Chabrier (2012), A new vision of giant planet interiors: Impact of double diffusive convection, *Astron. Astrophys.*, *540*, A20, doi:10.1051/0004-6361/201117595.
- Leconte, J., and G. Chabrier (2013), Layered convection as the origin of Saturn's luminosity anomaly, *Nat. Geosci.*, *6*(April), 347–350, doi:10.1038/ngeo1791.
- Ledoux, P. (1947), Stellar models with convection and with discontinuity of the mean molecular weight, *Astrophys. J. Lett.*, *105*, 305.
- Lenosky, T. J., S. R. Bickham, J. D. Kress, and L. A. Collins (2000), *Phys. Rev. B*, *61*, 1.
- Lodders, K. (2003), Solar system abundances and condensation temperatures of the elements, *Astrophys. J.*, *591*, 1220–1247.
- Lorenzen, W., B. Holst, and R. Redmer (2009), Demixing of hydrogen and helium at megabar pressures, *Phys. Rev. Lett.*, *102*, 115,701, doi:10.1103/PhysRevLett.102.115701.
- Lorenzen, W., B. Holst, and R. Redmer (2011), Metallization in hydrogen-helium mixtures, *Phys Rev B*, *84*, 235,109, doi:10.1103/PhysRevB.84.235109.
- Loubeyre, P., J. M. Besson, and J. P. Pinceaux (1982), High-Pressure Melting Curve of 4He, *Phys Rev Lett*, *49*(16), 1172–1175.
- Loubeyre, P., R. Le Toullec, and J. P. Pinceaux (1985), Helium compressional effect on H₂ molecules surrounded by dense H₂-He mixtures, *Phys Rev B*, *32*(11), 7611–7613.
- Loubeyre, P., R. Le Toullec, and J. P. Pinceaux (1987), Binary phase diagrams of H₂-He mixtures at high temperature and high pressure, *Phys Rev B*, *36*(7), 3723–3730.
- Magalhães, J. A., A. Seiff, and R. E. Young (2002), The stratification of Jupiter's Troposphere at the Galileo Probe Entry Site, *Icarus*, *158*, 410.
- Magro, W. R., D. M. Ceperley, C. Pierleoni, and B. Bernu (1996), *Phys. Rev. Lett.*, *76*, 1240.
- Militzer, B. (2005), *J. Low Temp. Phys.*, *139*, 739.
- Militzer, B. (2006), *Phys. Rev. Lett.*, *97*, 175,501.
- Militzer, B. (2009), *Phys. Rev. B*, *79*, 155,105.
- Militzer, B. (2013), *Phys. Rev. B*, *87*, 014,202.
- Militzer, B., and D. M. Ceperley (2000), *Phys. Rev. Lett.*, *85*, 1890.
- Militzer, B., and D. M. Ceperley (2001), *Phys. Rev. E*, *63*, 066,404.
- Militzer, B., and K. P. Driver (2015), *Phys. Rev. Lett.*, *115*, 176,403.
- Militzer, B., and R. L. Graham (2006), *Journal of Physics and Chemistry of Solids*, *67*, 2136.
- Militzer, B., and W. B. Hubbard (2007), *AIP Conf. Proc.*, *955*, 1395.
- Militzer, B., and W. B. Hubbard (2013), *Astrophys. J.*, *774*, 148.
- Militzer, B., W. H. Hubbard, J. Vorberger, I. Tamblyn, and S. A. Bonev (2008), *Astrophys. J. Lett.*, *688*, L45.
- Mirouh, G. M., P. Garaud, S. Stellmach, A. L. Traxler, and T. S. Wood (2012), a New Model for Mixing By Double-Diffusive Convection (Semi-Convection). I. the Conditions for Layer Formation, *Astrophys. J.*, *750*(1), 61, doi:10.1088/0004-637X/750/1/61.
- Mizuno, H., K. Nakazawa, and C. Hayashi (1978), Instability of a Gaseous Envelope Surrounding a Planetary Core and Formation of Giant Planets, *Prog. Theor. Phys.*, *60*(3), 699–710.
- Monserrat, B., N. D. Drummond, C. J. Pickard, and R. J. Needs (2014), *Phys. Rev. Lett.*, *112*, 055,504.
- Morales, M. A., C. Pierleoni, E. Schwegler, and D. M. Ceperley (2009), *Proc. Nat. Acad. Sci.*, *106*, 1324.
- Morales, M. A., C. Pierleoni, E. Schwegler, and D. M. Ceperley (2010), *Proc. Nat. Acad. Sci.*, *107*, 12,799.
- Morales, M. A., J. M. McMahon, C. Pierleoni, and D. M. Ceperley (2013), *Phys. Rev. Lett.*, *110*, 065,702.
- Mordasini, C. A., Y. Alibert, H. H. Klahr, and T. Henning (2012), Characterization of exoplanets from their formation. I. Models of combined planet formation and evolution, *Astron. Astrophys.*, *547*, A111, doi:10.1051/0004-6361/201118457.
- Nellis, W. J., N. C. Holmes, a. C. Mitchell, R. J. Trainor, G. K. Governo, M. Ross, and D. A. Young (1984), Shock Compression of Liquid Helium to 56 GPa, *PRL*, *53*(13), 1248.
- Nettelmann, N., B. Holst, A. Kietzmann, M. French, R. Redmer, and D. Blaschke (2008), *Astrophys. J.*, *683*, 1217.
- Nettelmann, N., A. Becker, B. Holst, and R. Redmer (2012), *Astrophys. J.*, *750*, 52.
- Nettelmann, N., J. J. Fortney, K. Moore, and C. Mankovich (2015), An exploration of double diffusive convection in Jupiter as a result of hydrogen-helium phase separation, *Mon. Not. R. Astron. Soc.*, *447*, 3422–3441, doi:10.1093/mnras/stu2634.
- Norman, G., and A. Starostin (1968), *Teplotophys. Vys. Temp.*, *6*, 410.

- Pfaffenzeller, O., D. Hohl, and P. Ballone (1995), *Phys. Rev. Lett.*, **74**, 2599.
- Pollack, J. B., O. Hubicky, P. Bodenheimer, and J. J. Lissauer (1996), Formation of the Giant Planets by Concurrent Accretion of Solids Gas, *Icarus*, **124**, 62–85, doi:10.1006/icar.1996.0190.
- Potekhin, A. Y., J. A. Pons, and D. Page (2015), Neutron Stars–Cooling and Transport Alexander, *Space Sci. Rev.*, **191**(1), 239, doi:10.1007/978-1-4939-3550-5.
- Radko, T. (2003), A mechanism for layer formation in a double-diffusive fluid, *J. Fluid Mech.*, **497**, 365–380, doi:10.1017/S0022112003006785.
- Rankine, W. J. M. (1870), On the thermodynamic theory of waves of finite longitudinal disturbances, *Philosophical Transactions of the Royal Society of London*, **160**, 277.
- Rogers, F. (1986), *Astrophys. J.*, **310**, 723.
- Rosenblum, E., P. Garaud, A. Traxler, and S. Stellmach (2011), Turbulent Mixing and Layer Formation in Double-Diffusive Convection: Three-Dimensional Numerical Simulations and Theory, *Astrophys. J.*, **731**(1), 66, doi:10.1088/0004-637X/731/1/66.
- Ross, M. (1998), *Phys. Rev. B*, **58**, 669.
- Rutten, R. J. (2003), *Radiative transfer in stellar atmospheres*, 8th edition ed., Utrecht University lecture notes.
- Saumon, D., and G. Chabrier (1992), *Phys. Rev. A*, **46**, 2084.
- Saumon, D., and T. Guillot (2004), *Astrophys. J.*, **609**, 1170.
- Saumon, D., G. Chabrier, and H. M. V. Horn (1995), *Astrophys. J. Suppl.*, **99**, 713.
- Schouten, J. A., L. C. Van den Bergh, and N. J. Trappeniers (1985), Demixing in a molecular hydrogen-helium mixture up to 50 kbar, *Chem. Phys. Lett.*, **114**(4), 401–404.
- Seiff, A., D. B. Kirk, T. C. D. Knight, R. E. Young, J. D. Mihalov, L. A. Young, F. S. Milos, G. Schubert, R. C. Blanchard, and D. Atkinson (1998), Thermal structure of jupiter's atmosphere near the edge of a 5- μ m hot spot in the north equatorial belt, *J. Geophys. Res.*, **103**, 22,857.
- Soubiran, F., and B. Militzer (2015), Miscibility calculations for water and hydrogen in giant planets, *Astrophys. J.*, **806**, 228.
- Soubiran, F., and B. Militzer (2016), The Properties of Heavy Elements in Giant Planet Envelopes, *Astrophys. J.*, *in press*, <http://arxiv.org/abs/1606.04162>.
- Soubiran, F., S. Mazevet, C. Winisdoerffer, and G. Chabrier (2012), Helium gap in the warm dense matter regime and experimental reflectivity measurements, *Phys. Rev. B - Condens. Matter Mater. Phys.*, **86**, 115,102, doi:10.1103/PhysRevB.86.115102.
- Soubiran, F., S. Mazevet, C. Winisdoerffer, and G. Chabrier (2013), *Phys. Rev. B*, **87**, 165,114.
- Spruit, H. C. (2013), Semiconvection: theory, *Astron. Astrophys.*, **552**, A76, doi:10.1051/0004-6361/201220575.
- Stern, M. E. (1960), The Salt-Fountain and Thermohaline Convection, *Tellus*, **12**(2), 172–175, doi:10.1111/j.2153-3490.1960.tb01295.x.
- Stevenson, D. (1985), Cosmochemistry and structure of the giant planets and their satellites, *Icarus*, **62**, 4–15, doi:10.1016/0019-1035(85)90168-X.
- Stevenson, D., and E. Salpeter (1977a), *Astrophys. J. Suppl. Ser.*, **35**, 221.
- Stevenson, D., and E. Salpeter (1977b), *Astrophys. J. Suppl.*, **35**, 239.
- Stevenson, D. J. (1982), Interiors of the Giant Planets, *Annu. Rev. Earth Planet. Sci.*, **10**, 257–295.
- Streett, W. B. (1973), Phase equilibria in molecular hydrogen-helium mixtures at high pressures, *Astrophys. J.*, **186**, 1107.
- Vorberger, J., I. Tamblyn, B. Militzer, and S. Bonev (2007), *Phys. Rev. B*, **75**, 024,206.
- Vos, W. L., M. G. E. Van Hinsberg, and J. a. Schouten (1990), High-pressure triple point in helium: The melting line of helium up to 240 kbar, *Phys. Rev. B*, **42**(10), 6106–6109, doi:10.1103/PhysRevB.42.6106.
- Wahl, S., W. B. Hubbard, and B. Militzer (2016a), The concentric maclaurin spheroid method with tides and a rotational enhancement of saturn's tidal response, *Icarus*, *submitted*, <http://arxiv.org/abs/1602.07350>.
- Wahl, S., W. B. Hubbard, and B. Militzer (2016b), Tidal response of preliminary jupiter model, *Astrophys. J.*, *in press*, <http://arxiv.org/abs/1607.08559>.
- Wahl, S. M., H. F. Wilson, and B. Militzer (2013), *Astrophys. J.*, **773**, 95.
- Weir, S., A. Mitchell, and W. Nellis (1996), *Phys. Rev. Lett.*, **76**, 1860.
- Wilson, H. F., and B. Militzer (2010), *Phys. Rev. Lett.*, **104**, 121,101.
- Wilson, H. F., and B. Militzer (2012a), Solubility of Water Ice in Metallic Hydrogen: Consequences for Core Erosion in Gas Giant Planets, *Astrophys. J.*, **745**(1), 54, doi:10.1088/0004-637X/745/1/54.
- Wilson, H. F., and B. Militzer (2012b), Rocky Core Solubility in Jupiter and Giant Exoplanets, *Phys. Rev. Lett.*, **108**(11), 111,101, doi:10.1103/PhysRevLett.108.111101.
- Winisdoerffer, C., and G. Chabrier (2005), Free-energy model for fluid helium at high density, *Phys. Rev. E - Stat. Nonlinear, Soft Matter Phys.*, **71**, 026,402, doi:10.1103/PhysRevE.71.026402.
- Wisdom, J., and W. B. Hubbard (2016), Differential rotation in Jupiter: A comparison of methods, *Icarus*, **267**, 315–322, doi:10.1016/j.icarus.2015.12.030.
- Wong, M., P. R. Mahaffy, S. K. Atreya, H. B. Niemann, and T. C. Owen (2004), Updated galileo probe mass spectrometer measurements of carbon, oxygen, nitrogen, and sulfur on jupiter, *Icarus*, **171**, 153–170.
- Wood, T. S., P. Garaud, and S. Stellmach (2013), A New Model for Mixing By Double-Diffusive Convection (Semi-Convection). II. The Transport of Heat and Composition Through Layers, *Astrophys. J.*, **768**(2), 157, doi:10.1088/0004-637X/768/2/157.
- Zeldovich, Y. B., and Y. P. Raizer (1968), *Elements of Gasdynamics and the Classical Theory of Shock Waves*, Academic Press, New York.
- Zharkov, V. N., and V. P. Trubitsyn (1978), *Physics of Planetary Interiors*, Pachart, Tucson.